LEGIBILITY NOTICE

A major purpose of the Technical Information Center is to provide the broadest dissemination possible of information contained in DOE's Research and Development Reports to business, industry, the academic community, and federal, state and local governments.

Although a small portion of this report is not reproducible, it is being made available to expedite the availability of information on the research discussed herein.

LA-UR -86-3852

Los Alamos National Laboratory is operated by the University of California for the United States Department of Energy under contract W-7405-ENG-36

LA-UR--86-3852

DE87 002907

TITLE GROWTH OF BUCKLING INSTABILITIES DURING RADIAL COLLAPSE OF AN IMPULSIVELY-LOADED CYLINDERICAL SHELL

AUTHOR(S) T. A. Duffey, R. H. Warnes, and J. M. Greene

SUBMITTED TO Fifth National Congress on Pressure Vessels and Piping

DISCLAIMER

Los Alamos National Laboratory
Los Alamos, New Mexico 87545

GROWTH OF BUCKLING INSTABILITIES DURING RADIAL COLLAPSE OF AN IMPULSIVELY-LOADED CYLINDRICAL SHELL

by

T. A. Duffey, R. H. Warnes, and J. M. Greene

ABSTRACT

Conditions leading to the growth of initial imperfections for rings or cylindrical shells subjected to initial uniform inward impulsive velocity loading are investigated. The work is motivated by a need to prevent buckling of rings during the contracting ring test, which is used to determine intermediate strain rate compressive stress-strain data. A previous analysis by Abrahamson is extended to include deceleration of the ring during inward motion; and the results of this deceleration are found to greatly influence the growth of imperfections (buckling). Qualitative comparisons with experimental data are presented.

I. INTRODUCTION

There have been a number of practical engineering applications that require the uniform radial collapse of simple structures, particularly cylindrical and spherical shells. Such applications include, for example, magnetic flux compression devices for generating large magnetic fields, explosive closure devices for rapidly sealing off pipes, and contracting ring tests for determining material properties at intermediate strain rates. In all applications of which the authors have knowledge, the goal of the device requires the prevention of buckling of the structure during inward motion.

The work reported herein was motivated by a need to prevent observed buckling of the contracting thin ring as it is being driven radially inward during the contracting ring test. The presence of buckling invalidated the determination of stress-strain behavior from the test; and it was hoped that an understanding of growth of such instabilities might lead to a modified design capable of substantial radius reductions without buckling.

A wealth of papers are available on the plastic buckling of cylindrical shells subjected to impulsive pressure loading, and the work is extensively reviewed in Ref. 1. Unfortunately, most of the work is of little use in predicting the buckling behavior of cylindrical shells undergoing radial collapse since no account of the significant shell thickening is considered. However, two papers do include such shell thickening.[2,3] It is shown in these papers that increase in thickness during significant inward motion of a cylindrical shell improves stability of the shell; and that at sufficiently high collapse velocities, the buckling will be negligible.

Considered in Refs. 2, 3 is the case of constant collapse velocity only. This assumption may serve to approximate the case of some highly overdriven shells for which material strength is unimportant. However, for the case of the contracting ring test, the uniform component of inward velocity decreases substantially during inward motion, and the contracting shell may come to rest before complete collapse. As a result, the time available for growth of initial imperfections is increased, and the concept of a "critical" initial velocity no longer provides the entire pic're for "sufficiently stable" inward shell motions.[2]

It is the purpose of this paper to quantify the influence of shell deceleration on growth of instabilities during inward motion. In the next section, the principles behind the earlier buckling analysis by Abrahamson[2] are briefly reviewed and extended to include ring deceleration. In Section III, limited experimental data are presented, taken from contracting ring tests. Calculations using the new theory are presented and compared (to the extent possible) with the experimental data. Finally, conclusions (Section IV) are presented. A simple closed-form solution for the mean inward cylinder motion is presented in the Appendix.

II. DETAILS OF BUCKLING ANALYSIS AND REPRESENTATIVE RESULTS

Consider a ring subjected to uniform inward radial motion due to some large initial velocity, v_o. As discussed in Refs. 2-4, if no variations or imperfections in the geometry, material, or impulsive loading of the problem are present, the ring will move inward in a uniform manner, maintaining its circular shape, until the initial kinetic energy is fully absorbed as plastic

work in the ring. Assuming that the ring material is incompressible, the ring will become progressively thicker on continued inward motion.

However, due to inevitable imperfections in geometry, material properties, and loading, this uniform, radially inward motion will be perturbed. The situation is depicted in Fig. 1, taken from Ref. 4, where a small part of the ring lags behind the remainder of the ring. Because of the presence of the compressive circumferential stress in the ring, the tendency will be for this location to lag behind the overall inward ring motion even more. The curvature of the ring is increased at this location.[2,3]

For a perfectly plastic material, the flow stress is constant, so the perturbational increase in curvature causes no bending moment. There is thus no resistance to the perturbation, and the perturbation grows, resulting in unstable motion.[2,3]

With the introduction of strain hardening, point B (Fig.1) has a somewhat larger strain than point A due to the local change in curvature at the perturbation location, and there results a restoring moment opposing the action of the compressive circumferential stress.[2,3] The situation is analogous to that of the curved beam shown in Fig. 2.

Growth of the displacement perturbation in Fig. 2 is enhanced by the compressive axial membrane stress (proportional to h) and opposed by the presence of a restoring bending moment caused by a differential bending stress

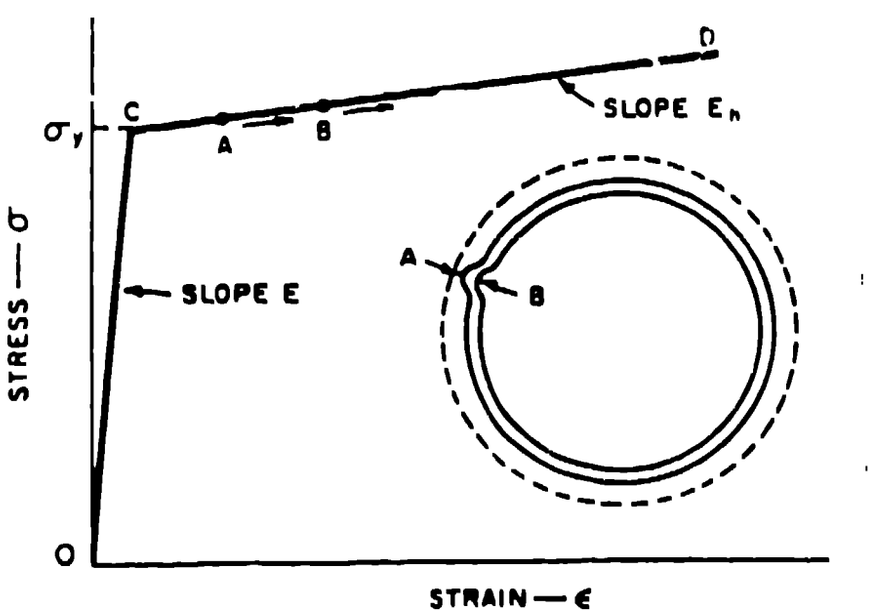

Fig. 1. Perturbed Motion of Contracting Ring (from Ref. 4).

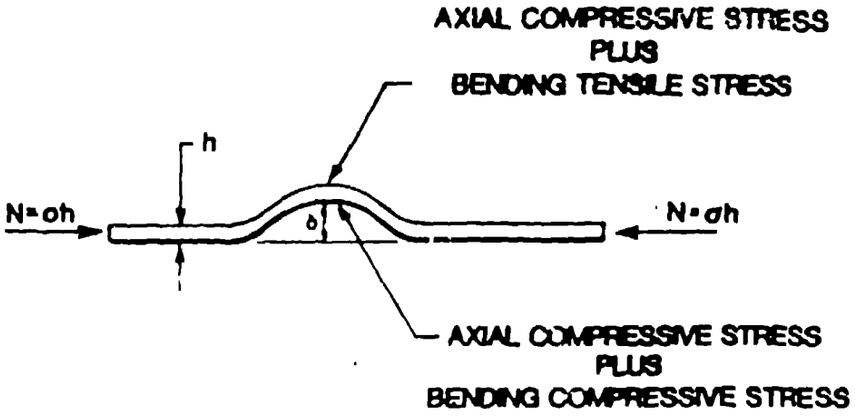

Fig. 2. Curved Beam Analogue.

across the beam cross-section (proportional to h^3), tension on the top surface and compression on the bottom surface.

Now due to large inward unperturbed displacements of the ring or cylinder, thickening of the shell occurs. Because of thickening, both thrust and resistive motion of the perturbed state increase: thrust proportional to thickness, and resistive motion proportional to thickness cubed. Therefore, stability improves as inward motion proceeds. A given unstable mode may then become stable upon inward motion.[2-4]

By writing the equations of motion of the ring in terms of perturbed and unperturbed displacements and their spatial derivatives, it is shown in Refs. 2, 4 that instability growth is governed by the following second order ordinary differential equation:

$$\xi^6 \ddot{f}_n + (n^2-1)(n^2-s^2\xi^4)f_n = s^2\xi^4(n^2-1) \qquad (1)$$

with initial conditions $f_n(o)=\dot{f}_n(o)=o$

The following definitions apply:

$\xi = \frac{r}{r_o}$, where r_o is original mean radius, and r is current mean radius;

n = mode number of initial departure from circularity and buckling displacement (initial departure from circularity and growth of buckling displacement are assumed to be represented by a countably infinite series of normal displacement modes, n = 2, ...,);

f_n = Amplification function associated with the nth mode growth. It is the ratio of the maximum amplitude of the nth mode at a given time to the initial amplitude of the shape imperfection associated with the nth mode. Thus a value of f_n = 100 means that the nth mode shape has grown to a value of 100 times its initial imperfection amplitude;

$s^2 = 12\left(\frac{r_o}{h_o}\right)^2 \frac{\bar{\sigma}}{E_h}$, where h_o is initial shell thickness, E_h is the strain hardening modulus* of the stress-strain curve (see Fig. 1), and $\bar{\sigma}$ is a mean stress.* Finally, ($\dot{}$) denotes time derivative with respect to nondimensional time, τ,

$\tau = aC_h t/r_o$, where

$a^2 = h_o^2/12r_o^2$; $C_h = \sqrt{\frac{E_h}{\rho}}$, where ρ is mass density; and t is real time.

In Refs. 2 and 4, Eq. (1) is solved numerically for each mode assuming inward shell velocity, $\dot{\xi}$ = constant. In the following, this restriction is removed.

---

*E_h is assumed small, so that $\bar{\sigma}$ - a constant; but finite, so that there is a restoring moment.

It can be shown that, in terms of the nondimensional parameters previously defined, the unperturbed, purely inward radial motion is given by (for compressive stress assumed positive):

$$\ddot{\xi} = \frac{s^2}{\xi} \tag{2}$$

subject to the initial conditions, $\xi(0) = 1$; $\dot{\xi}(0) = \frac{-V_o}{aC_h}$, where V_o is initial impulsive shell velocity (assumed spatially uniform).

Equations (1) and (2) can be interpreted as a general initial value problem,

$$\underline{y}' = \underline{f}(\underline{y}),$$

$\underline{y}(0) = \underline{y}_o$, where

$$\begin{Bmatrix} y_1' \\ y_2' \\ y_3' \\ y_4' \end{Bmatrix} = \begin{Bmatrix} y_2 \\ \frac{s^2}{y_1} \\ y_4 \\ \frac{(1-n^2)}{y_1^6}(n^2 - s^2 y_1^4) y_3 + \frac{s^2}{y_1^2}(n^2-1) \end{Bmatrix} \tag{3}$$

and where $y_1 = \xi$ $\quad y_3 = f_n$

$y_2 = \dot{\xi}$ $\quad y_4 = \dot{f}_n$

and

$$\begin{Bmatrix} (y_1)_o \\ (y_2)_o \\ (y_3)_o \\ (y_4)_o \end{Bmatrix} = \begin{Bmatrix} 1 \\ \frac{-V_o}{aCh} \\ 0 \\ 0 \end{Bmatrix} \tag{4}$$

The above system was solved using a generalized fourth-order Runge-Kutta method. For each mode*, $2 \leq n < s$, the above initial value problem was solved in time until one of the following three events occurred:

1. Initially unstable growth,

$$n^2 - s^2\xi^4 < 0 \qquad \text{(See Eq. (1))}, \tag{5}$$

becomes stable. Again, this stability change is due to shell thickening, and occurs at a nondimensional radius of

$$(\xi)_{stable} = \sqrt{\frac{n}{s}} \tag{6}$$

*Mode numbers $n = 0$, 1 do not contribute to growth of bending instability.

2. Inward motion of the ring ceases, that is,

$$\dot{\xi} = 0$$

3. Total collapse of the ring occurs.

Note that all modes for which $n \geq s$ are always stable, since ξ initially equals unity and monotonically decreases toward zero with time. This can be seen from either Eq. (1) or (5).

From Eq. (1), it can also be seen that growth of instabilities is of a nature exponential in time.

Calculations based upon the above are performed for the following values of the geometry - material parameter, s: 15, 30, 60, 100, and 150. This range in s covers a wide and representative range of ring radius-to-thickness ratios and material properties. Results are presented in Figs. 3-7, respectively. For clarity, only selected modes are presented (every other mode for s = 15, 30; and every fourth mode for s = 60, 100, and 150). Generic behavior for each mode in Figs. 3-7 is shown in Fig. 8. Normalized instability growth, f_n, is plotted as the ordinate. This is the amplification function for the nth mode growth and, again, is the ratio of amplitude of the nth mode at a given time to the initial amplitude of the shape imperfection for that mode. Normalized uniform initial velocity imparted to the ring is plotted as the abscissa.

Two intersecting branches are observed for generic mode n in Fig. 8 (as well as for all plotted modes in Figs. 3-7). At the lower initial ring velocities, instability growth is terminated by cessation of inward ring motion, caused by inclusion of material strength for uniform inward motion.* When inward motion ceases, unloading occurs; and with the absence of a compressive in-plane force, there is no further tendency for buckling growth.

At higher ring velocities, mode n becomes stable due to ring thickening. At the point of intersection of the two curves, inward uniform (n=0) shell motion ceases at the instant the "stable thickness" of that particular mode is reached.

*Such material strength and resultant ring deceleration is neglected in Refs. 2-4.

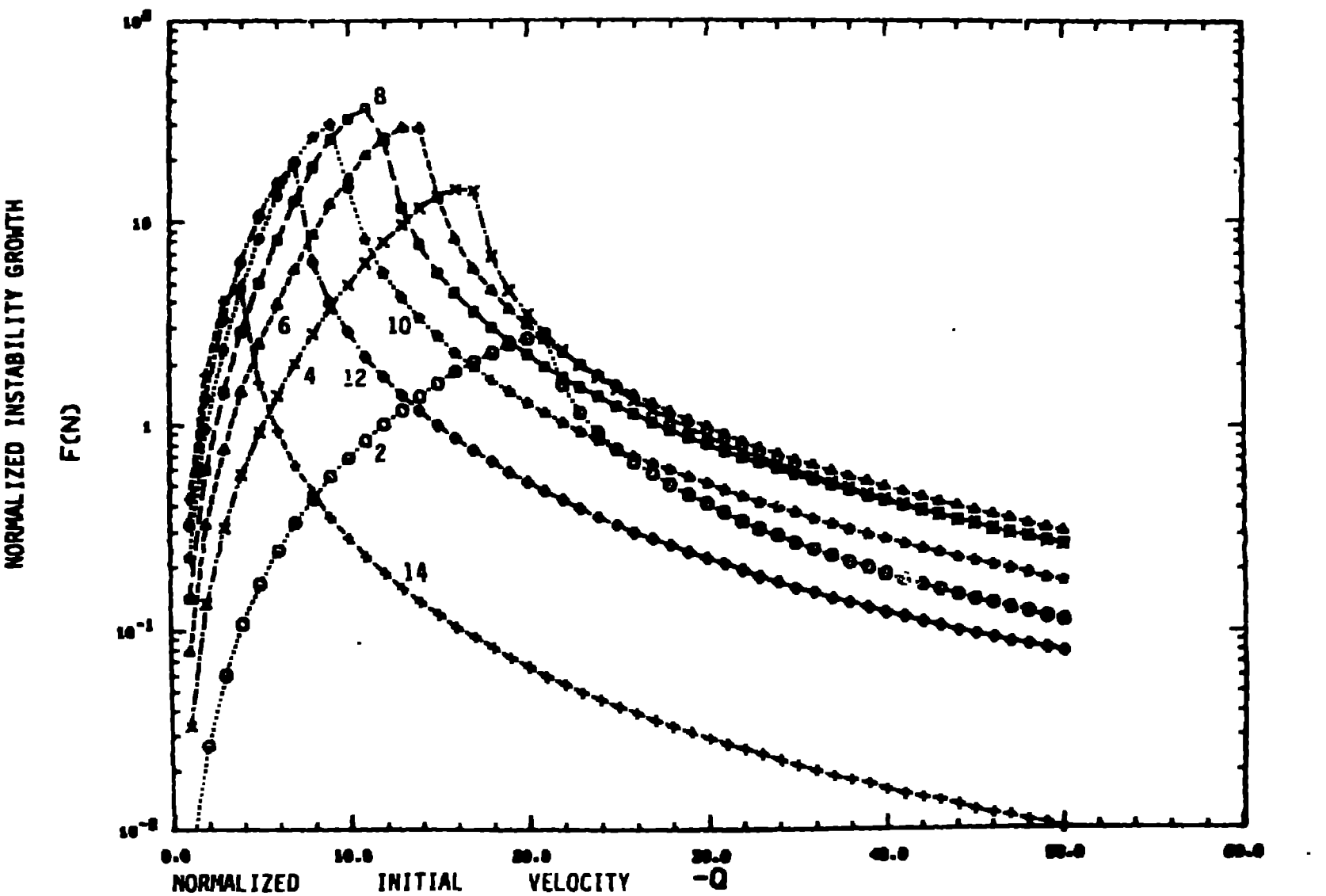

Fig. 3. Instability Growth for S=15. Every Other Mode Plotted.

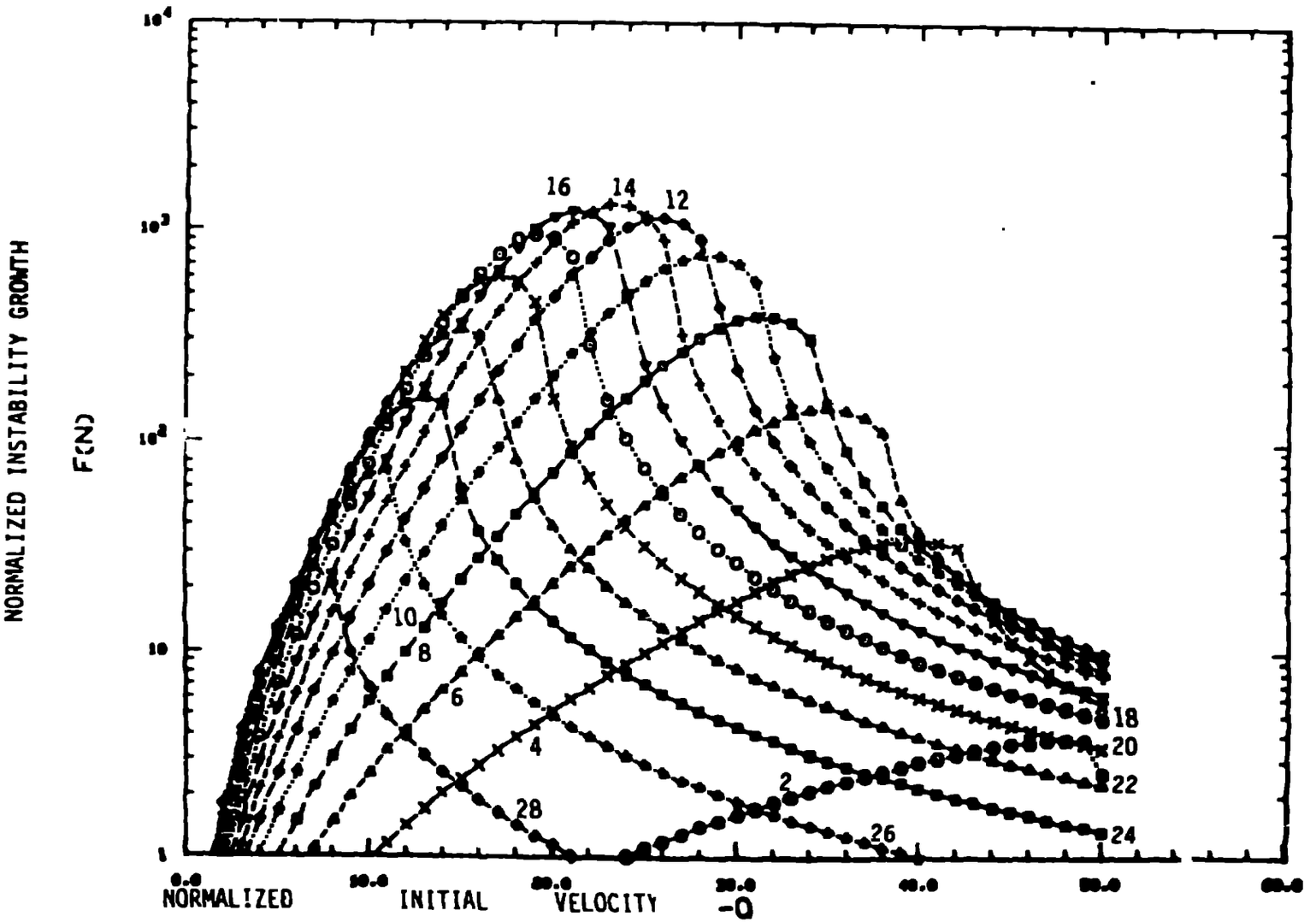

Fig. 4. Instability Growth for S=30. Every Other Mode Plotted.

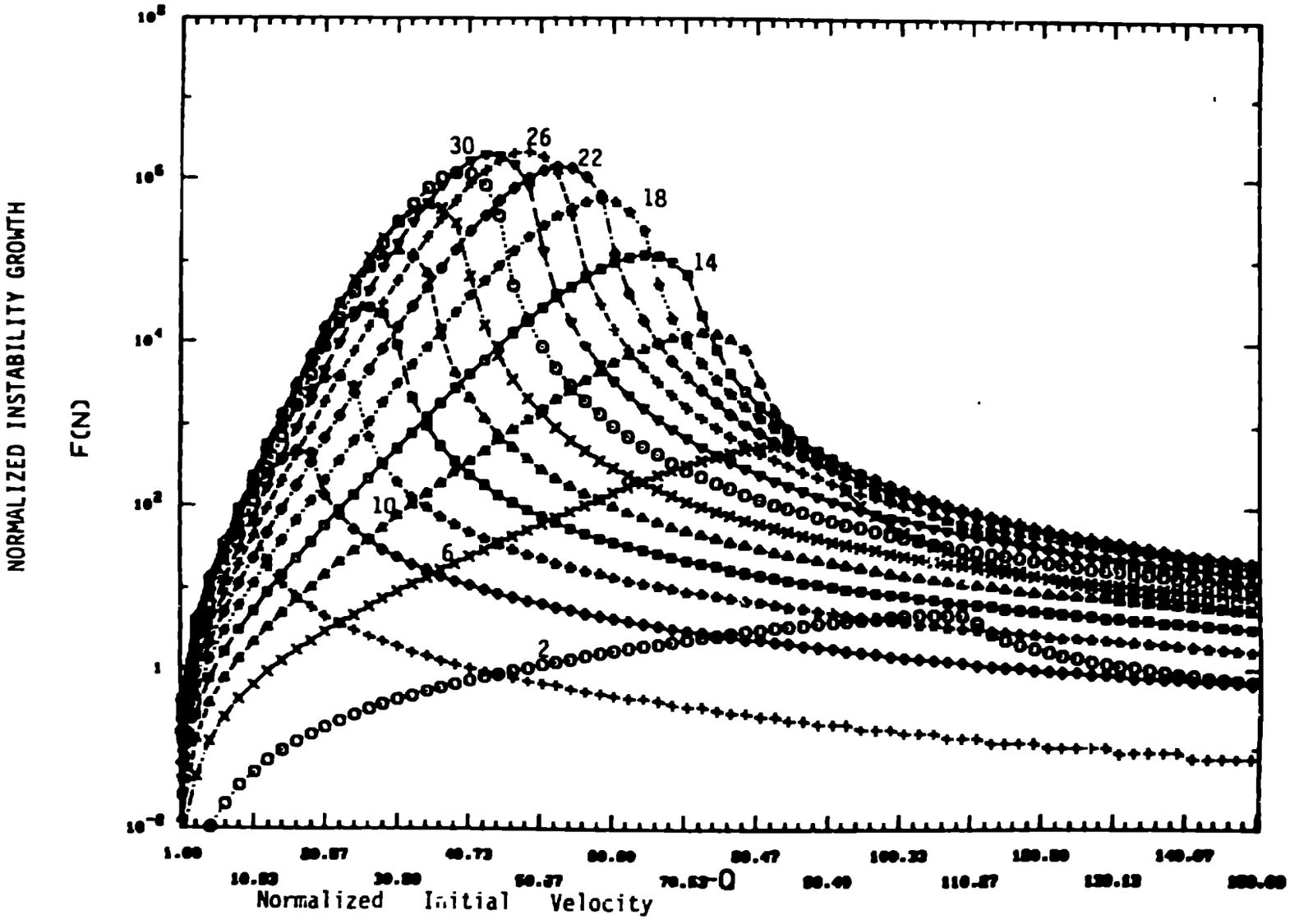

Fig. 5. Instability Growth for S=60. Every Fourth Mode Plotted.

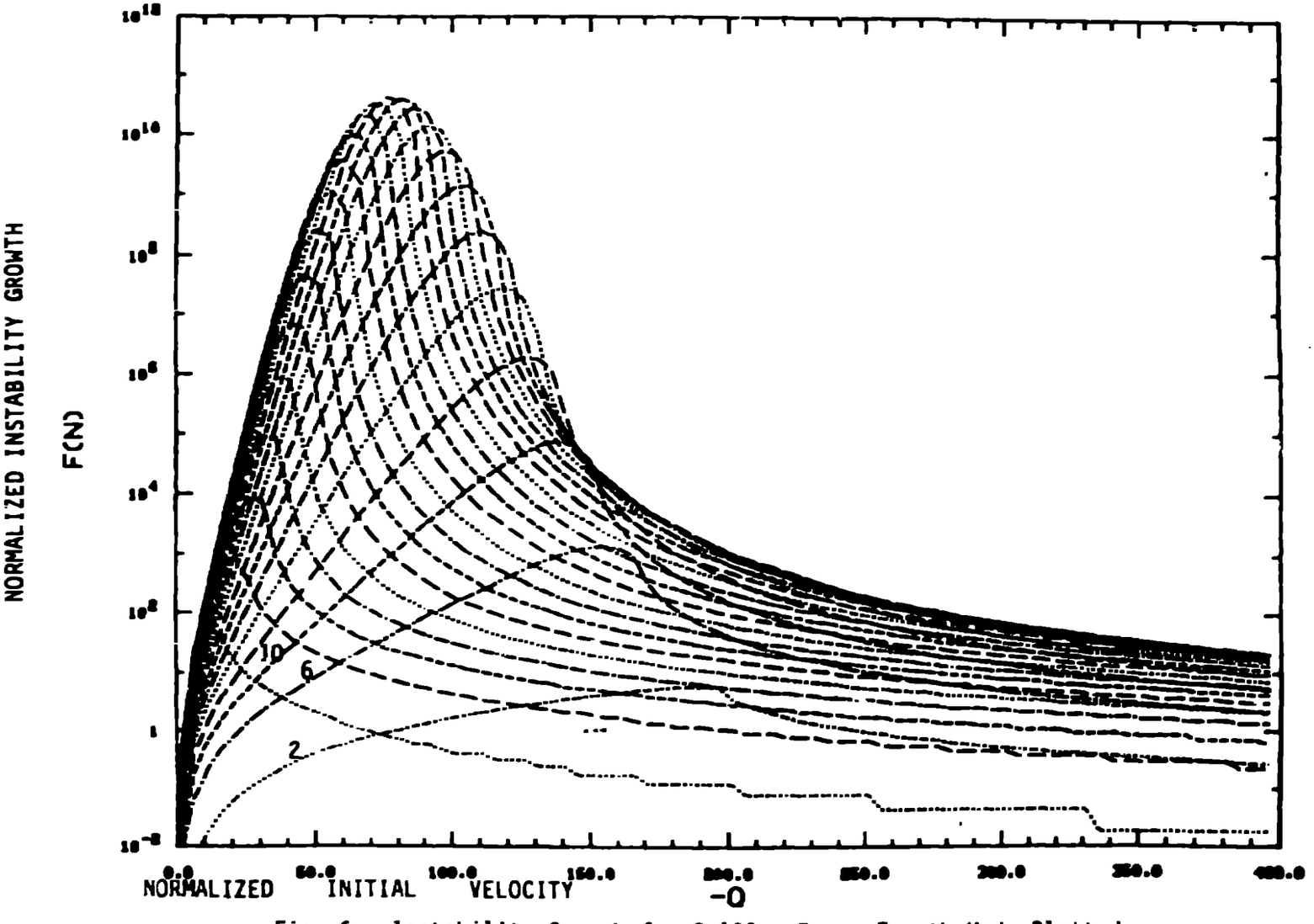

Fig. 6. Instability Growth for S=100. Every Fourth Mode Plotted.

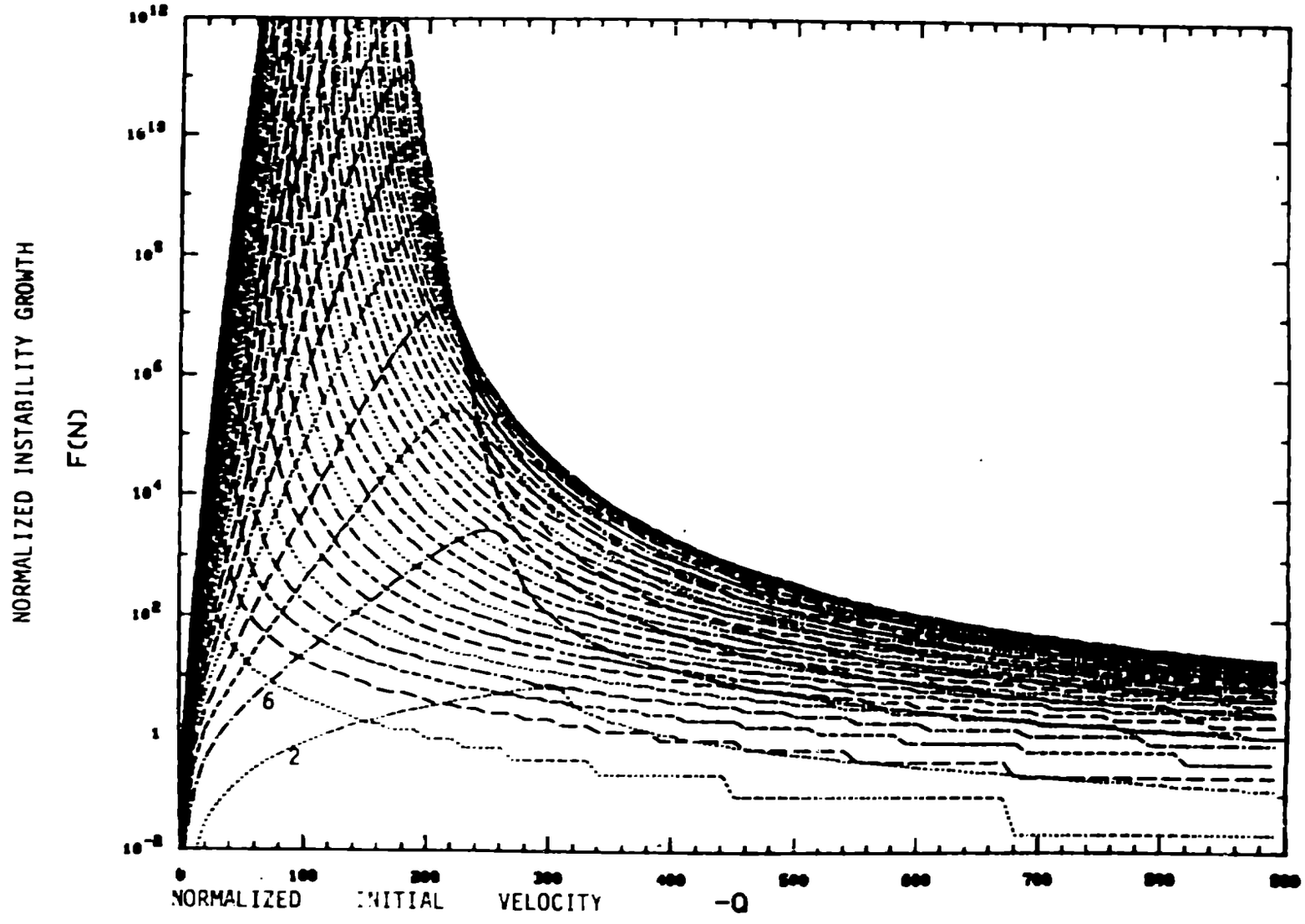

Fig. 7. Instability Growth for S=150. Every Fourth Mode Plotted.

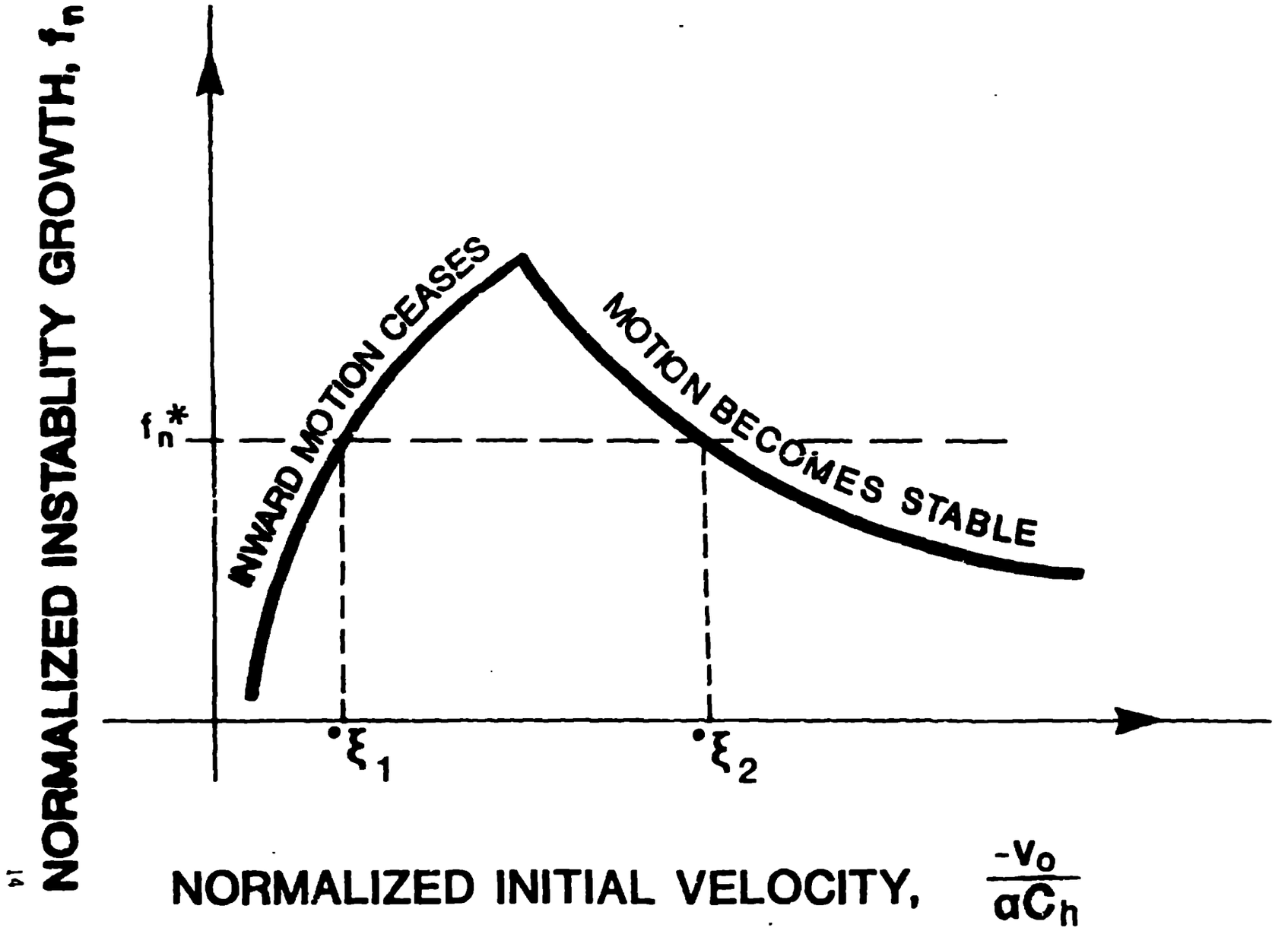

Fig. 8. Ring Behavior as a Function of Velocity for Generic Mode n.

Concentrating on mode n in Fig. 8, say that a maximum instability growth, f_n^*, can be tolerated (perhaps a value[2-4] of 10 or 100). Then a horizontal line drawn in Fig. 8 for that particular mode n reveals that growth of the instability remains acceptable as long as the initial (normalized) velocity either remains below $\dot{\xi}_1$, or above $\dot{\xi}_2$.

The situation in Figs. 3-7 is similar, but the most dominant mode depends upon the value of f_n^* selected. Also, for a given f_n^*, the dominant mode on the first branch ("inward motion ceases") is different from the dominant mode for the second branch ("motion becomes stable").

III. COMPARISONS OF RESULTS WITH EXPERIMENTAL DATA

A number of experiments have been performed in an attempt to uniformly drive a thin metal ring radially inward. The intent of the experimental program was to obtain compressive stress-strain mechanical material properties.* While some success was had at recording and interpreting ring motion, buckling was observed to develop rather early in the response of the ring, limiting the useful strain range over which data could be obtained.

Experiments were performed with one of two driving mechanisms: explosive or magnetic. A total of seven experiments was initially performed using high explosive ignited by a series of circumferentially placed detonators. The velocity of a point on the inside surface of each ring was recorded as a function of time using a velocity interferometer. Results suggested the possibility of buckling. However, no samples from these tests were recovered, nor were high-speed framing camera measurements of the overall motion taken.

A second set of explosively driven ring tests was performed on two rings to look specifically at buckling using a high-speed camera. One of these tests was highly successful in illustrating the onset and growth of the buckling shape during inward ring motion. One typical frame recorded is included in Fig. 9, and illustrates development of the buckling pattern.

*The experiments are effectively the inverse of the expanding ring tests, described in Ref. 5, and used to obtain dynamic tensile mechanical properties.

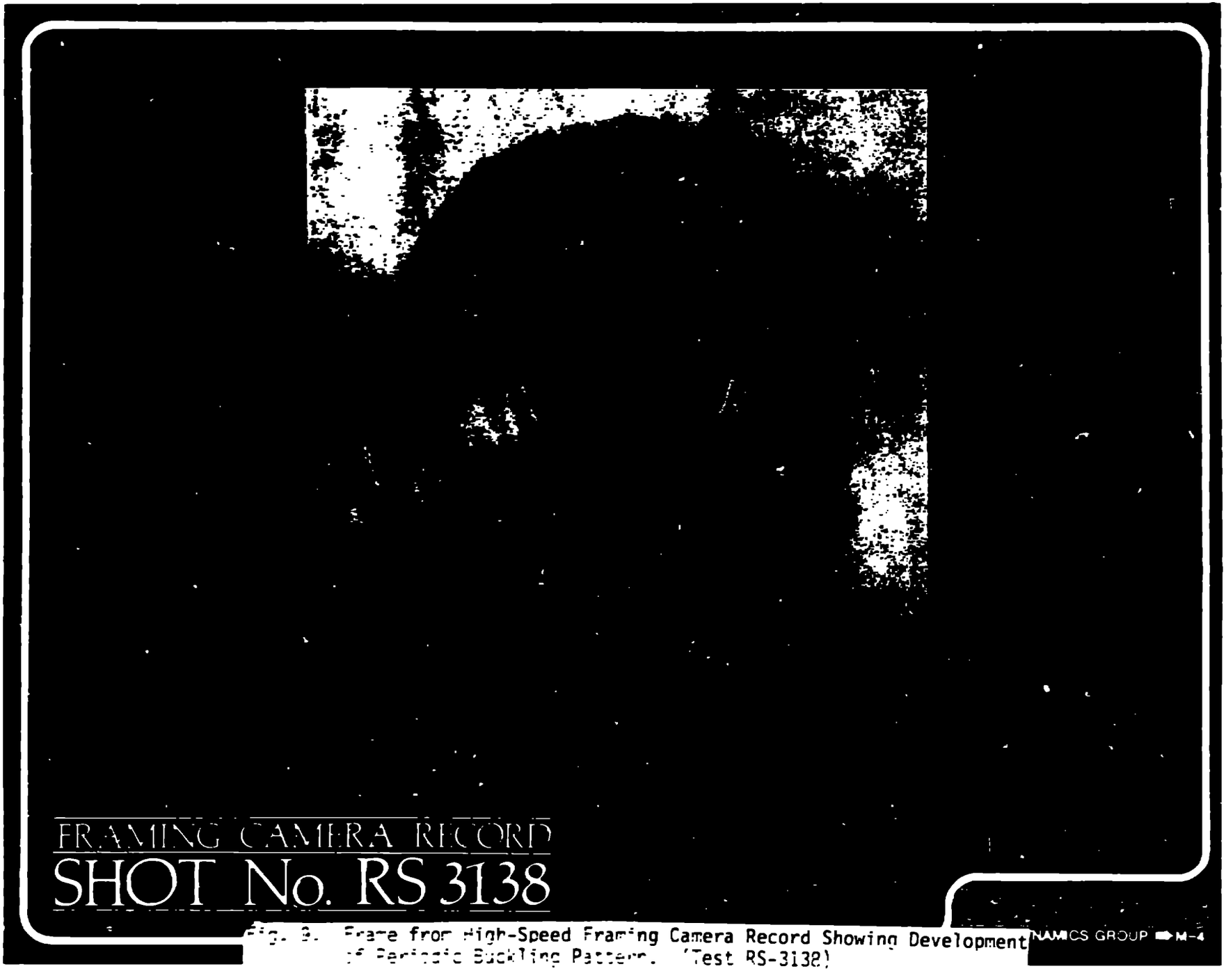

Fig. 9. Frame from High-Speed Framing Camera Record Showing Development of Periodic Buckling Pattern. (Test RS-3138)

Six ring tests were performed using the magnetic driving system. While no photographic coverage was undertaken, specimens on these tests were recovered either partially or fully intact. These post-test specimens are illustrated in Fig. 10. All rings underwent extensive buckling.

Experimental details of the seven ring tests potentially useful to this buckling study (the one explosively driven ring with photographic coverage, and the six magnetically driven rings) are indicated in Table I. In that table, the "initial velocity" indicated was determined as follows: For RS-3138 (explosive driving system), differentiation of framing camera data was used to determine the velocity as the ring left the driver; and for the remaining six magnetically driven rings listed in Table I, velocity interferometer data were used. The magnetic system caused a finite acceleration of the ring up to a maximum velocity. The "initial velocity" indicated for these tests is actually the maximum velocity achieved by the ring.

Noting that all rings were 6061-T6 aluminum, values for mean plastic stress, $\bar{\sigma}$, and slope of the strain hardening curve, E_h, were taken as follows Ref. 4. $\bar{\sigma}$ = 44000 psi; E_h = 1.3 x 10^5 psi.

Also, $\rho = 2.5 \times 10^{-4}$ lbf-sec^2/in^4.

Values of

$$s = 12\left(\frac{r_o}{h_o}\right)^2\left(\frac{\bar{\sigma}}{E_h}\right) \quad \text{and} \quad \frac{-V_o}{\alpha C_h}, \text{ where}$$

$$\alpha = \sqrt{\frac{h_o^2}{12r_o^2}} \quad \text{and} \quad C_h = \sqrt{\frac{E_h}{\rho}}$$

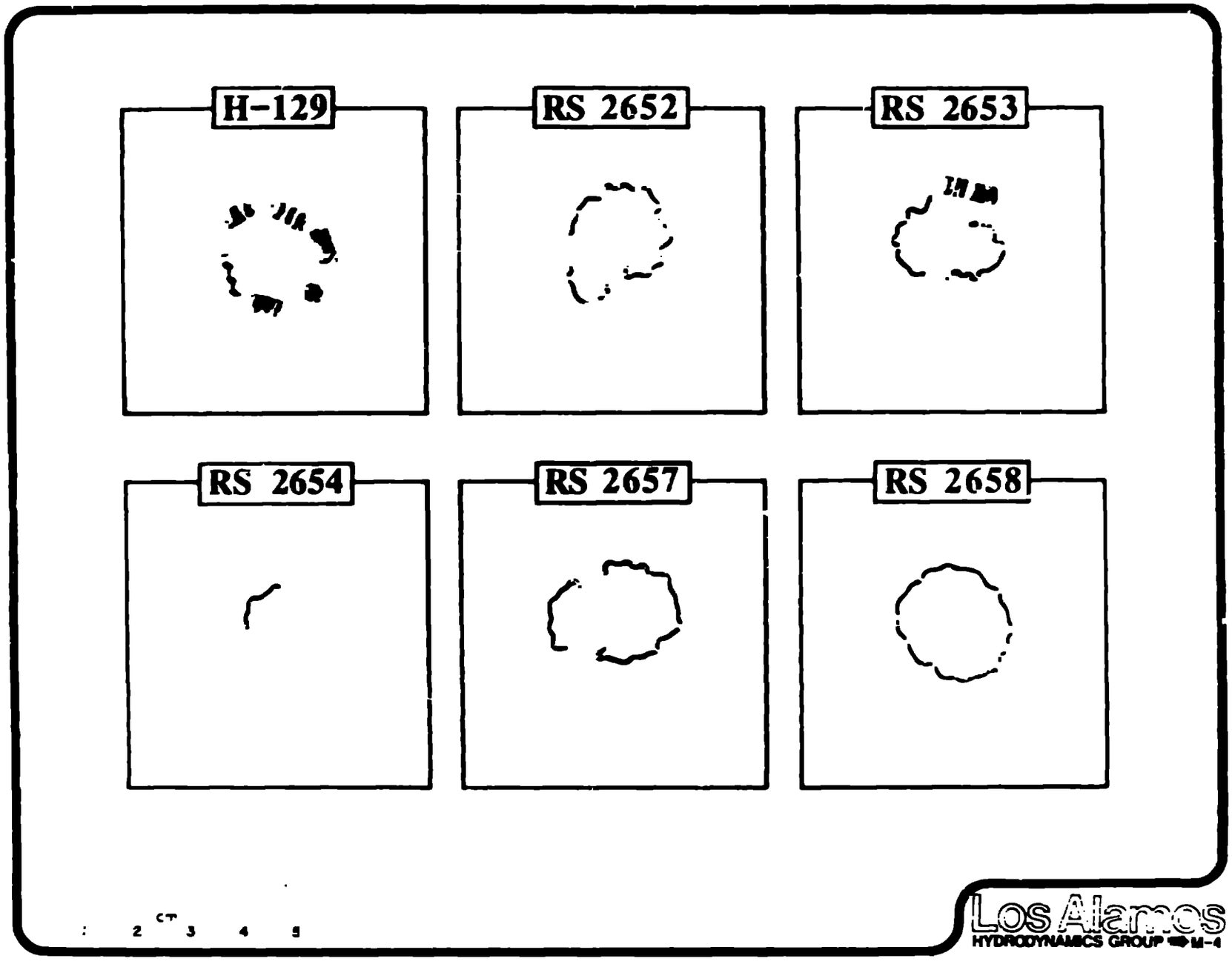

Fig. 10. Photograph of recovered pieces of magnetically-driven ring samples.

TABLE I
EXPERIMENTAL DETAILS OF IMPLODED RINGS USED IN BUCKLING STUDY

TEST ID	DRIVING SYSTEM	MATERIAL	(h_o) THICKNESS (IN)	MEAN (r_o) RADIUS (IN)	INITIAL VELOCITY (V) IN/SEC	DOMINANT MODE	COMMENTS
RS-3138	EXPLOSIVE	6061T6 AL	0.0315	0.4847	13779.5	n~14	n is approx. Half of ring hard to see. High speed camera data only.
RS-2652	MAGNETIC	6061-T6 AL	0.0258	0.4840	6299.2	n=16	Sample recovered.
RS-2653	MAGNETIC	6061-T6 AL	0.0280	0.4860	9448.8	n=16	Sample recovered
RS-2654	MAGNETIC	6061-T6 AL	0.0270	0.4865	9291.3	--	Ring not fully recovered.
RS-2657	MAGNETIC	6061-T6 AL	0.02935	0.4860	6299.2	n=15	Sample recovered.
RS-2658	MAGNETIC	6061-T6 AL	0.0289	0.4855	5314.9	n=15	Sample recovered
n-129	MAGNETIC	6061-T6	---	---	---	--	Ring not fully recovered.

were then calculated for each ring. Results of these evaluations are presented in Table II. Test H-129 has been omitted due to incomplete data. From Table II, there is some variation in geometry, and considerable variation in initial nondimensional velocity.

Next, calculations of buckling growth for the rings were performed using the theory in the previous section. Since values of s were reasonably close together, results of values near s = 31 are plotted in Fig. 11, and results of values near s = 38 are plotted in Fig. 12. Results reveal that all magnetically driven tests lie in the region where inward motion ceases, causing termination of buckling growth; whereas the one explosively driven ring (RS-3138) is near the intersection of the two branches of the growth curve. All six experiments lie in high buckling growth regions (all are above a nondimensional growth of 100), qualitatively agreeing with the observed significant observed buckling. However, the following two points are worth noting:

1. The initial impulsive velocity assumed in the analysis, while considered reasonable for the explosively driven ring, is definitely an approximation in the case of the five magnetic tests correlated. This approximation is due to the finite time over which the ring accelerates in this type of test.

2. Calculations are <u>extremely sensitive</u> upon the parameters, such as s.

With the above limitations in mind, however, it appears that growth of initial imperfections (buckling) can be limited by either dropping or raising the initial ring velocity or making a geometry and/or material change (i.e., a change in the value of the parameter, s). The particular parameters selected do not fall in a low buckling growth region.

IV. CONCLUSIONS AND RECOMMENDATIONS

A buckling theory originally developed by Abrahamson for collapsing rings and cylindrical shells (including thickening) has been extended to account for shell decelerations. Growth of initial displacement imperfections is found to be substantially modified; and instability growth can be limited

Table II

CALCULATED BUCKLING PARAMETERS FOR EACH EXPERIMENT

TEST ID	$a/h = r_o/h_o$	s	α	$-\frac{V_o}{\alpha C_h}$
RS-3138	15.4	31.0	0.0188	32.1
RS-2652	18.75	37.8	0.0154	17.9
RS-2653	17.35	35.0	0.0166	25.0
RS-2654	18.0	36.3	0.0160	25.5
RS-2657	16.5	33.3	0.0175	15.8
RS-2658	16.8	33.9	0.0172	13.6

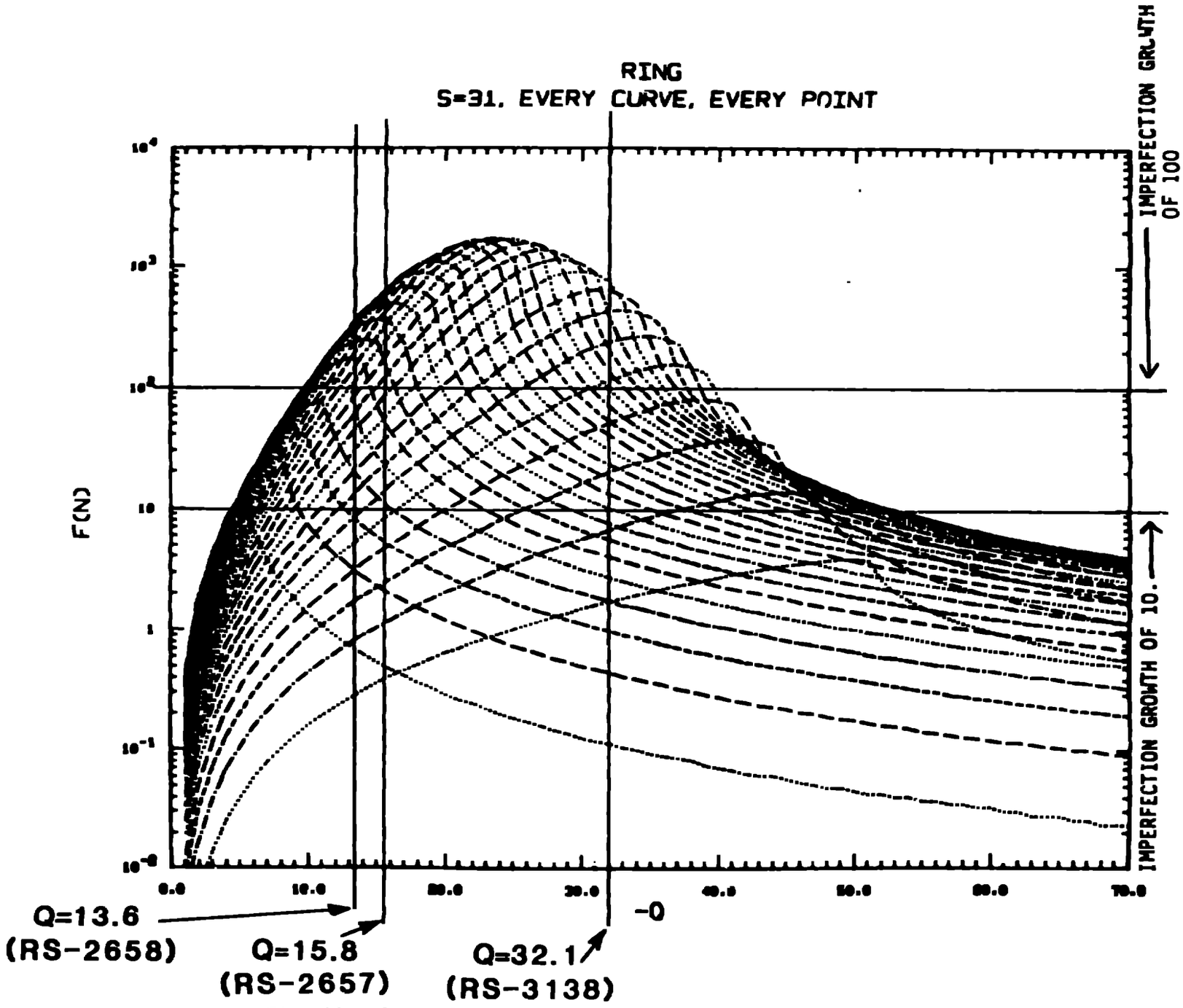

Fig 11. Instability Growth for Experimental Configurations, S=31.

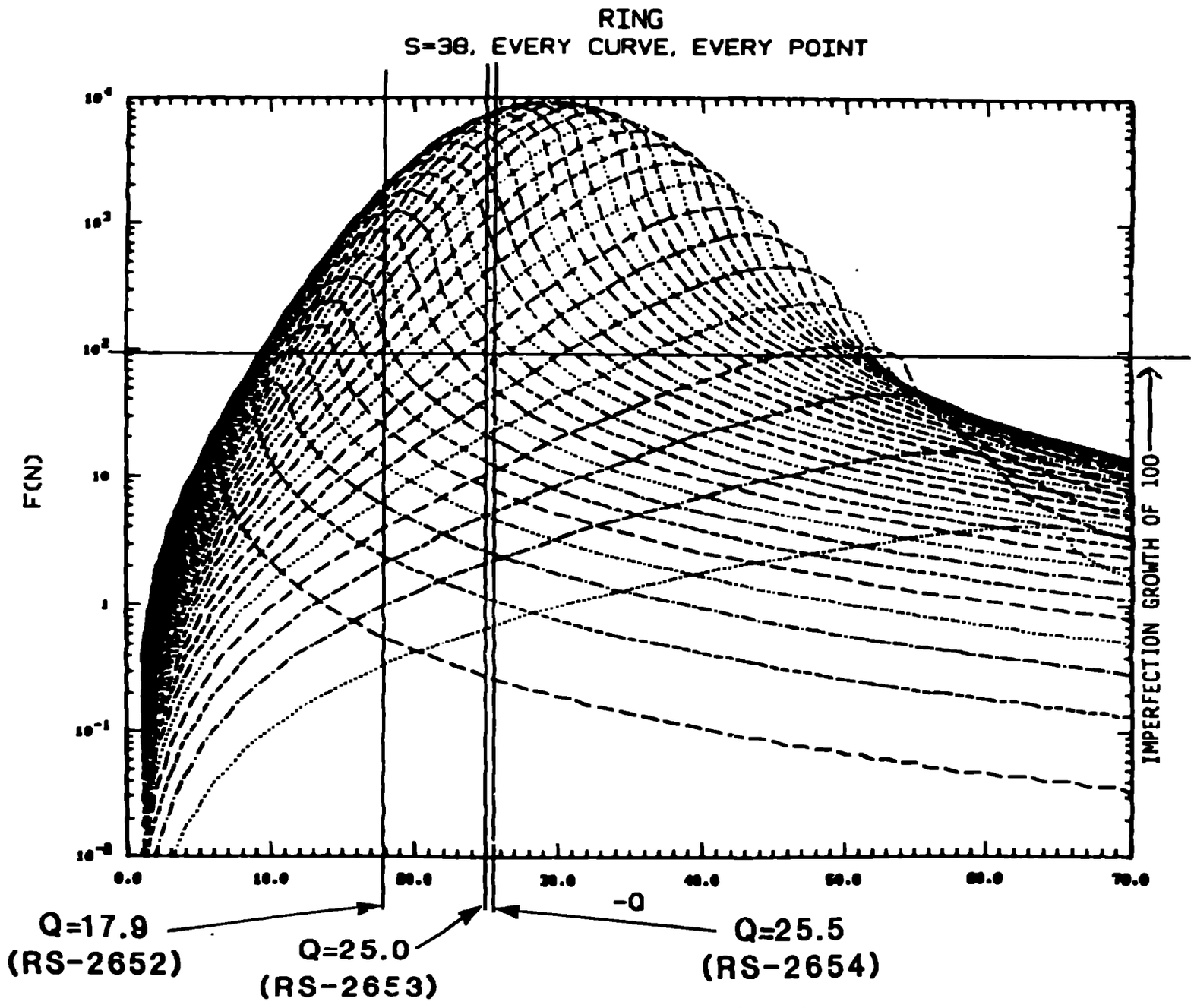

Fig. 12. Instability Growth for Experimental Configurations, S=38

by driving rings inward at either low or high velocities. Maximum imperfection growth appears in an intermediate velocity region.

Contracting ring tests performed using either an explosive or magnetic driving system are found to lie within the high growth region in all cases, in qualitative agreement with the observed extreme buckling growth.

ACKNOWLEDGEMENT

We wish to thank Elaine Alei for developing the plotting routines and computing the final results.

REFERENCES

1. N. Jones, "Response of Structures to Dynamic Loading," Institute of Physics Conference Series, No. 47, pp. 254-276, London, 1979.

2. G. R. Abrahamson, "Critical Velocity for Collapse of a Shell of Circular Cross Section Without Buckling," Journal of Applied Mechanics, June 1974, pp. 407-411.

3. A. L. Florence and G. R. Abrahamson, "Critical Velocity for Collapse of Viscoplastic Cylindrical Shells Without Buckling," Journal of Applied Mechanics, Vol. 44, No. 1, March 1977, pp. 89-94.

4. H. E. Lindberg and A. L. Florence, Dynamic Pulse Buckling - Theory and Experiment, DNA-6503H, Defense Nuclear Agency, Washington, D.C., February, 1983.

5. R. H. Warnes, et al., Development of the Freely Expanding Ring Test For Measuring Dynamic Material Properties, Proceedings, 1982 Spring Meeting, Society of Experimental Stress Analysis, Honolulu, Hawaii, pp. 656-661.

APPENDIX

SIMPLE SOLUTION FOR MEAN CYLINDER MOTION

A simple closed-form solution is presented for uniform inward ring motion. The solution is useful for checking results obtained numerically for the complete buckling analysis.

Beginning with Eq. (2),

$$\frac{d^2\xi}{d\tau^2} = \frac{s^2}{\xi} \tag{A.1}$$

subject to the initial conditions

$$\xi(0) = 1 \quad \text{and} \quad \frac{d\xi}{d\tau}(0) = -\frac{V_o}{aC_h}$$

where $\tau = aC_h t/r_o$, and other quantities are previously defined, let

$$\eta = \frac{d\xi}{d\tau}$$

Then $$\frac{d^2\xi}{d\tau^2} = \frac{d\eta}{d\tau} = \frac{d\eta}{d\xi}\frac{d\xi}{d\tau} = \eta\frac{d\eta}{d\xi} \tag{A.2}$$

Then Eq. (A.1) becomes

$$\eta\frac{d\eta}{d\xi} = \frac{s^2}{\xi} \tag{A.3}$$

Equation (A.3) can be integrated by separation of variables, resulting in

$$\frac{\eta^2}{2} = s^2 \ln\xi + C \tag{A.4}$$

where C is a constant of integration. For the initial condition:

$$\eta(0) = \eta_o = -\frac{V_o}{aC_h} \quad \text{at } \xi(0) = 1,$$

$$\eta = \sqrt{\eta_o^2 + 2s^2 \ln\xi} \tag{A.5}$$

Equation (A.5) gives the nondimensional inward velocity as a function of nondimensional radius. Finally, the nondimensional radius at which the inward velocity goes to zero can be found from Eq. (A.5) as

$$\xi^* = e^{-\frac{\eta_o^2}{2s^2}} \tag{A.6}$$